Vibration Detection in Distributed Acoustic Sensor With Threshold-Based Technique: A Statistical View and Analysis

Huan Wu, Chao Shang, Kun Zhu, and Chao Lu

***Abstract*—Detecting vibrations with high probability and low false alarm probability is crucial for prompting distributed acoustic sensors (DASs) to real applications. It is known that detection performance mainly depends on signal-to-noise ratio (SNR) and many efforts have been made to improve it. However, the relationship between SNR and detection performance has not been quantitatively analyzed so far. Threshold-based vibration detection is a simple and commonly used technique, but how to set the decision threshold in DAS is still an open question. In this work, for the first time, we propose a model to quantify the relationship between SNR and detection performance and provide a method for setting the decision threshold. Firstly, we build a model to differentiate vibrations from the background noise based on their short-time average energy. This model reveals that setting decision threshold requires perfect knowledge of noise power, which is a difficult task in DAS since noise power varies frequently with time and position. To solve this problem, secondly, we propose a noise-irrelevant threshold setting method based on autocorrelation-energy. Finally, experimental validation is performed on a DAS system along 47.4km sensing fiber with 5m spatial resolution. Results of autocorrelation-energy-based method show 100% and 98.1% detection probability for two vibrations with 1.12×10^{-7} false alarm probability in a one-hour measurement period.**

***Index Terms*—Detection probability, distributed acoustic sensor (DAS), false alarm probability, false alarm rate, signal-to-noise ratio (SNR), threshold-based technique, vibration detection.**

I. Introduction

DISTRIBUTED optical fiber sensor (DOFS) is a non-intrusive sensing technology that has been attracting researchers from various areas in recent years. It uses thin glass optical fiber as both sensing element and transmission medium, and they are compatible to the ubiquitously deployed fiber system across the world for carrying Internet and telecom traffic. Distributed acoustic sensor (DAS) is a kind of DOFS that has the capability of detecting faint vibrations along tens of kilometers of sensing fiber with a high spatial resolution. It has been extensively investigated in many applications such as seismic detection [1], intrusion detection [2], and pipeline surveillance [3]. For all the applications, vibration detection is a fundamental task in DAS. When the vibration has a high signal-to-noise ratio (SNR), it can be easily distinguished since it obviously sticks out of the noise floor. However, there are several factors that may result in low SNR and make vibration detection practically challenging. First, the vibration signal may be quite weak due to the long distance between the vibration source and sensing fiber. Second, signal fading phenomena including interference-induced fading and polarization-induced fading in DAS make vibration detection more difficult [4]; Third, received signals are contaminated by unavoidable noise from DAS system and environment. DAS system noise can come from phase noise and frequency drift of the laser, finite extinction ratio (ER) of optical pulses, thermal noise from electrical components, amplified spontaneous emission (ASE) noise from the optical amplifier, and quantization noise from data acquisition. Environmental noise is mainly due to the ambient changes around sensing fiber and it may be serious for the fiber sections locating at habitually noisy environments such as residential areas. Due to the uncertainty of vibration signal and noise power, SNR of the vibration signal fluctuates randomly with different locations and moments.

To improve the SNR of vibration signals in DAS, different hardware and signal processing methods have been proposed. The original DAS was realized with direct detection [5], whose configuration is simple but SNR is quite low for long-distance sensing. Coherent detection scheme proposed in [6] greatly improves SNR due to the coherent amplification effect. Raman and Brillouin amplification are also introduced to further improve SNR and extend the sensing range [7], [8]. To alleviate polarization-induced and interference-induced fading, polarization diversity scheme [9] and multi-frequency acquisition scheme [10] have been proposed. Besides hardware modification schemes, different kinds of signal processing methods have also been extensively studied to improve SNR. Time-domain noise reduction methods such as moving average [6] and transform

Manuscript received September 24, 2020; revised October 31, 2020; accepted November 2, 2020. Date of publication November 6, 2020; date of current version June 16, 2021. This work was supported in part by the National Key Research and Development Program of China under Grant 2018YFB1801701, in part by the National Natural Science Foundation of China (NSFC) under Grant U1701661, and in part by The Hong Kong Polytechnic University PolyU under Grant H-ZG7E. *(Corresponding author: Kun Zhu.)*

Huan Wu and Kun Zhu are with the Department of Electronic and Information Engineering, The Hong Kong Polytechnic University, Kowloon, Hong Kong (e-mail: hkpolyu.wu@polyu.edu.hk; zker@zju.edu.cn).

Chao Lu is with the Department of Electronic and Information Engineering, The Hong Kong Polytechnic University, Kowloon, Hong Kong, and also with the Hong Kong Polytechnic University Shenzhen Research Institute, Shenzhen 518057, China (e-mail: enluchao@polyu.edu.hk).

Chao Shang is with the Key Laboratory of Luminescence and Optical Information (Ministry of Education), Institute of Optical Information, School of Science, Beijing Jiaotong University, Beijing 100044, China (e-mail: cshang@bjtu.edu.cn).

Color versions of one or more of the figures in this article are available online at https://ieeexplore.ieee.org.

Digital Object Identifier 10.1109/JLT.2020.3036450

TABLE I
CONFUSION MATRIX OF FOUR POSSIBLE TYPES OF RESPONSE IN VIBRATION DETECTION

Actual \ Response	Yes	No
vibration present	Detect P_d	Miss $1-P_d$
vibration absent	False alarm (FA) P_{fa}	Correct rejection $1-P_{fa}$

domain denoising methods such as wavelet shrinkage in [11] are popular algorithms to reduce noise in DAS. To fully utilize DAS information, two-dimensional signal processing methods like edge detection [12] and bilateral filtering [13] are also proposed. Even though all the above methods can be used for SNR improvement in DAS, none of the aforementioned methods has indicated the relationship between SNR and vibration detection performance. Intuitively, a high SNR will bring a high vibration detection probability. However, it is still unknown to what extent SNR improvement will bring a 100% guaranteed detection. Thus, a quantitative analysis of the relationship between SNR and detection performance is essential for DAS system design and evaluation.

The function of vibration detection in DAS is to decide whether the vibration is present or absent during a specific time period for every position along sensing fiber. The confusion matrix of four possible types of response is summarized in Table I. When a "Yes" response is given to a vibration present scenario, it is a correct response and called a "Detect"; but when a "Yes" response is given to a vibration absent scenario, it is a mistake and called a "False alarm" ("FA"). Similarly, when a "no" response is given to a vibration present case, it is a mistake and called a "Miss"; but when a "no" response is given to a vibration absent case, it is correct and called a "Correct rejection". Since the proportion of "Detect" and "FA" provide all information in the data, detector performance can be evaluated by P_d (the probability of "Detect") and P_{fa}, (the probability of "FA"). A vibration detector with high false alarm probability or low detection probability will hinder the practical usage of a DAS system. For example, a DAS system with even 100% detection probability but 30% false alarm probability can hardly be used. Therefore, the optimization of a vibration detector consists in minimizing false alarm probability and maximizing detection probability.

Different techniques can be adopted for vibration detection in DAS. A straightforward and commonly used technique is comparing an extracted feature with a decision threshold [14]–[18]. A vibration signal is supposed to be present if it is higher than the decision threshold; Otherwise, if it is lower than the decision threshold, a vibration signal is regarded as absent. There is an obvious trade-off between setting a higher decision threshold to reduce false alarm probability and a lower decision threshold to increase detection probability. The feature can be extracted from different descriptive attributes, such as level crossing rate (LCR) [14], kurtosis [15], peak-to-peak value [16], and short-time average energy [17], [18]. A classical signal detection method was proposed by Urkowitz in 1967 by measuring short-time average energy [19]. The basic idea is that with the presence of a signal, the energy would be significantly larger compared with the scenario of no signal present. This method is simple and easy to use because it requires no prior information about the signal to be detected. For a pipeline integrity threat detection DAS system, the short-time average energy is compared with the empirical threshold values to decide the presence of vibrations [18]. The empirical threshold values are set between 1 to 40 times average background noise energy for different positions. But theoretically, there are no explicit rules to set the exact value of the threshold, which is essential for the practical DAS applications.

In this work, to the best of our knowledge, it is the first time that a quantitative relationship between SNR and detection performance is derived and guidance on decision threshold setting is provided.

1) We build a model to discriminate the vibration signal from background noise based on their short-time average energy. Threshold setting rule based on a target false alarm rate (FAR) in DAS is proposed and relationships among detection performance, SNR, and processing window size are quantitatively studied.
2) For the average-energy-based method, setting decision threshold requires prior knowledge of noise power which is hard to be estimated in DAS. To solve this problem, we propose a noise-irrelevant threshold setting method based on autocorrelation-energy. Three factors affecting detection performance are quantitatively analyzed.
3) Both the average-energy-based method and autocorrelation-energy-based method are demonstrated on a DAS system of 47.4km long sensing fiber with 5m spatial resolution. Unlike the threshold is highly dependent on the accuracy of noise estimation with average-energy-based method, with autocorrelation-energy based method, vibration detection with a single threshold is feasible without noise estimation. A DAS system with 100% and 98.1% detection probabilities for two vibrations and 1.12×10^{-7} false alarm probability within a one-hour measurement period is presented.

The rest of the paper is organized as follows: data structure and data processing of DAS are introduced in Section II. Vibration detection based on average energy is presented in Section III. Vibration detection based on autocorrelation-energy is proposed in Section IV. Experimental results and discussions are given in Section V. Finally, the conclusion is drawn in Section VI.

II. DATA STRUCTURE AND DATA PROCESSING OF DAS

A. Data Structure of DAS

The working principle of DAS is based on phase-sensitive OTDR utilizing the interference effect of Rayleigh backscattering (RBS) of different scattering centers within the pulse width. Fig. 1 shows the principle of a DAS system. Coherent optical pulses are sent into the fiber under test (FUT) through a circulator, a large number of scattering points within the pulse will interfere with each other and form a randomly interfered

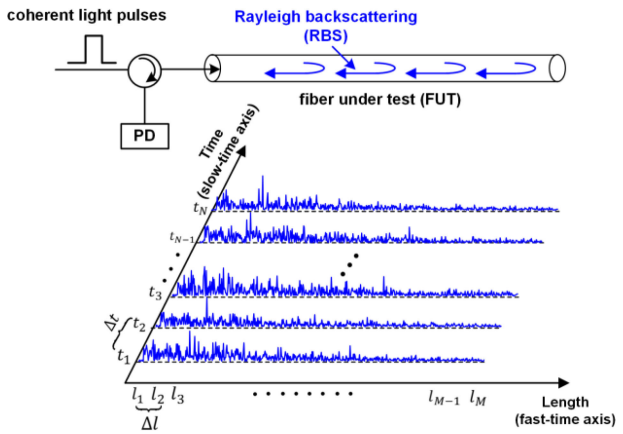

Fig. 1. Working principle and data structure of a DAS system.

RBS signal. The RBS traces are detected by a photodetector (PD) and recorded as a function of time. Collected raw data are organized in a two-dimensional structure as shown in Fig. 1. Axis along the fiber (also called fast-time axis) is used to discriminate position according to the speed of light while another axis along measurand in time (also called slow-time axis) is used to describe vibration in time series. The data can be expressed by matrix X[M, N],

$$X\left[M,N\right] = \begin{bmatrix} x_1^1 \cdots x_M^1 \\ \vdots \ddots \vdots \\ x_1^N \cdots x_M^N \end{bmatrix} \tag{1}$$

where x_m^n represents RBS amplitude at position l_m and time t_n. M is the number of sampling points along the FUT, which is determined by the sampling rate of data acquisition system and length of FUT. N is the number of recorded RBS traces, which is determined by pulse repetition rate and measurement period. In Fig. 1, position $l_m = m{*}\Delta l$, where $\Delta l = v_g/(2{*}sampling\ rate)$ is spatial sampling resolution, and time delay $t_n = n{*}\Delta t$, where $\Delta t = 1/pulse\ repetition\ rate\ (Hz)$ is the pulse period. Since the RBS traces are affected by DAS system noise and environmental noise, the data matrix can be expressed as $X[M,N] = S[\mathrm{M},\mathrm{N}] + W[\mathrm{M},\mathrm{N}]$, where $S[\mathrm{M},\mathrm{N}]$ and $W[M,N]$ are vibration signal matrix and noise matrix, respectively. With regard to the white noise after PD, RBS amplitudes along slow-time axis follow the Gaussian distribution [20].

B. Data Processing of DAS

After acquiring RBS traces, an intelligent data processing system that can automatically process data and provide useful knowledge for decision making is desirable. The workflow of data processing for DAS is shown in Fig. 2. Firstly, raw data are acquired after A/D converter and signal pre-processing such as digital filtering are performed. Due to the possible low SNR of the vibration signals, a specific signal enhancement algorithm may be used to improve SNR. Then the data are handed over to a feature extraction algorithm. Feature extractor I can locate certain components in signals to assist vibration detection. The

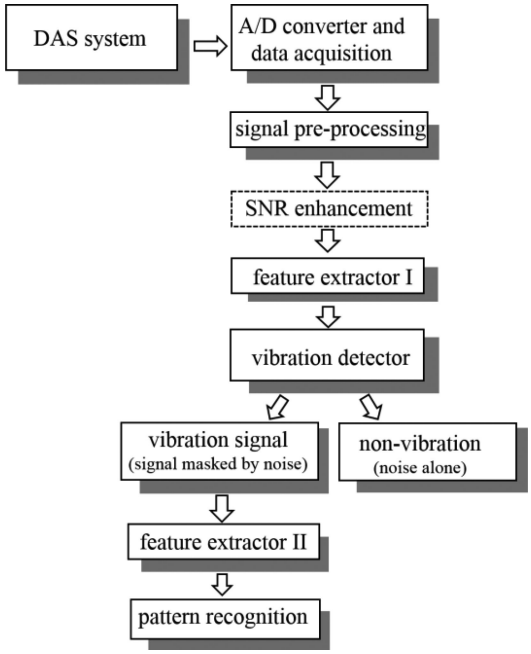

Fig. 2. Workflow of data processing in DAS.

vibration detector will decide whether the data is 'noise alone' or 'signal masked by noise'. If vibration detector declares that vibration signal exists, then detected vibrations go through pattern recognition stage. Features extracted by feature extractor II are statistically compared to either trained or fixed features to map them to a known set of event classes. In most cases, prior training is essential to initialize the classifier. Pattern recognition based on machine learning and deep learning is a recent trend in DAS [21], [22]. However, a DAS system continuously acquires numerous data in practical applications, it is difficult to implement real-time signal classification for every position along the FUT due to the limitations of data transmission and storage. A quick pre-selection of possible vibration positions must be carried out before pattern recognition, and the pre-selected vibration signals will be sent for further pattern recognition procedure. Mathematically, vibration detection and pattern recognition are called binary and multiclass hypothesis testing and their objective is to minimize decision errors. In this work, our focus is on vibration detection.

III. Vibration Detection Based on Average Energy Method

A. Theoretical Model

Mathematically, collected data at a specific position have two possible hypotheses:

$$\mathcal{H}_0 \ : \ x\ (n) = \ w\,(n) \tag{2a}$$

$$\mathcal{H}_1 \ : \ x\ (n) = \ s\,(n) + w\,(n) \tag{2b}$$

Hypothesis $\mathcal{H}_0$ is for the absence of vibration and Hypothesis $\mathcal{H}_1$ is for the presence of vibration. $s(n)$, $w(n)$ and $x(n)$ represent clean signal, noise and measured, respectively. Both the signal and noise are assumed to be an i.i.d. (independent

and identically distributed) Gaussian random process with zero mean and σ_s^2 and σ_w^2 variance, respectively. Signal-to-noise ratio (SNR) is defined as the ratio of signal power to noise power. For the zero-mean signal, the SNR is:

$$SNR = \frac{\sigma_s^2}{\sigma_w^2} \tag{3}$$

The short-time average energy of a measured signal, $x(n)$, with N_s samples can be expressed as:

$$\mu = \frac{1}{N_s} \sum_{n=0}^{N_s-1} x(n)^2 \tag{4}$$

The computed average energy will be compared with a pre-determined threshold λ to decide the signal's presence. It is obvious that different threshold values will give different signal presence information. To quantify the detection performance, statistical distribution of μ under Hypotheses $\mathcal{H}_0$ and $\mathcal{H}_1$ are analyzed. Since the sum of squares of N_s independent standard Gaussian random variables is a Chi-square random variable with N_s degrees of freedom (proof is given in *Appendix, Lemma1*), the test statistics μ is a random variable whose probability density function (PDF) is Chi-square distributed. Let us denote a Chi-square distributed random variable X with N_s degrees of freedom as $X \sim \chi^2_{N_s}$. It is clear that under Hypothesis $\mathcal{H}_0$, $N_s u/\sigma_w^2 \sim \chi^2_{N_s}$, and under $\mathcal{H}_1$ $N_s u/(\sigma_w^2+\sigma_s^2) \sim \chi^2_{N_s}$. Therefore, the PDF of test statistics u is:

$$f_u(\mu, N_s) \sim \begin{cases} \frac{\sigma_w^2}{N_s} f_\chi\left(\frac{\mu\sigma_w^2}{N_s}, N_s\right) & under\ \mathcal{H}_0 \\ \frac{\sigma_w^2+\sigma_s^2}{N_s} f_\chi\left(\frac{\mu(\sigma_w^2+\sigma_s^2)}{N_s}, N_s\right) & under\ \mathcal{H}_1 \end{cases} \tag{5}$$

Under $\mathcal{H}_0$, $E(u) = \sigma_w^2$ and $var(u) = \frac{2}{N_s}\sigma_w^4$; under $\mathcal{H}_1$ $E(u) = \sigma_w^2 + \sigma_s^2$, $var(u) = \frac{2}{N_s}(\sigma_w^2+\sigma_s^2)^2$ (Proof is given in *Appendix Lemma2*). According to the central limit theorem [24], when independent random variables are added, their distributions tend toward Gaussian even if the original variables themselves are not Gaussian distributed. Therefore, test statistics u asymptotically obeys the Gaussian distribution as:

$$f_u(\mu, N_s) \sim \begin{cases} N\left(\sigma_w^2, \frac{2}{N_s}\sigma_w^4\right) & under\ \mathcal{H}_0 \\ N\left(\sigma_w^2+\sigma_s^2, \frac{2}{N_s}(\sigma_w^2+\sigma_s^2)^4\right) & under\ \mathcal{H}_1 \end{cases} \tag{6}$$

where $N(\alpha, \beta)$ represents Gaussian distribution with meanα and variance β.

As mentioned in Introduction, two probabilities are of interest for vibration detection, i.e.,

1) the detection probability, P_d, which defines the probability of vibration detector having detected the presence of vibration under $\mathcal{H}_1$.
2) the false alarm probability, P_{fa}, which defines, the probability of the vibration detector claiming the presence of vibration under $\mathcal{H}_0$.

For a given threshold λ, false alarm probability is given by:

$$P_{fa}(\lambda) = P[u > \lambda\ \mathcal{H}_0] = Q\left(\frac{\lambda - \sigma_w^2}{\sigma_w^2/\sqrt{N_s/2}}\right) \tag{7}$$

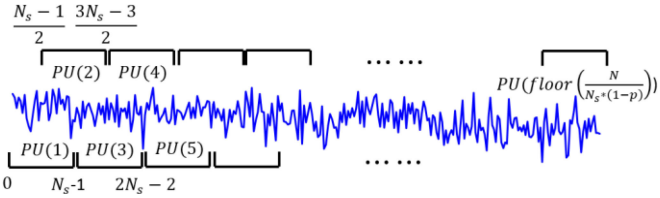

Fig. 3. Illustration of processing units with 50% overlap for position l_m.

where $Q(x)$ is the tail distribution function of standard Gaussian distribution as, $Q(x) = \int_x^\infty \frac{1}{\sqrt{2\pi}} e^{-t^2/2}\, dt$. $Q^{-1}(x)$ represents the inverse function of $Q(x)$. To decide whether a vibration signal is present, we need to set a threshold for the average energy level. In most cases, it is not easy to set this threshold value based on the detection probability since we have little or no prior knowledge about the vibration signal. An alternative is to set the threshold based on false alarm probability under $\mathcal{H}_0$ by inverting (7):

$$\lambda_{fa} = \sigma_w^2 \left(1 + \frac{Q^{-1}(P_{fa})}{\sqrt{N_s/2}}\right) \tag{8}$$

When the threshold is set to λ_{fa}, the detection probability P_d is given by:

$$P_d(\lambda_{fa}) = P[u > \lambda_{fa}\ \mathcal{H}_1] = Q\left(\frac{\lambda_{fa} - (\sigma_w^2+\sigma_s^2)}{(\sigma_w^2+\sigma_s^2)/\sqrt{N_s/2}}\right) \tag{9}$$

B. Average-Energy-Based Method for Vibration Detection in DAS

As depicted in Section II, the collected RBS traces can be decomposed into a matrix. For a specific position l_m along the FUT, N_s adjacent points (i.e., processing window size) along the slow-time axis are accumulated as one processing unit (PU) to calculate average energy,

$$\mu(l_m, 0 : N_s - 1) = \frac{1}{N_s} \sum_{n=0}^{N_s-1} (x_m^n)^2 \tag{10}$$

If average energy is computed with p (in %) overlap, then the total number of PU along the FUT within t_N measurement period is $floor(\frac{N}{N_s*(1-p)}) * M$. Fig. 3 gives an illustration of PU blocks with half overlap ($p = 50\%$).

According to the theoretical analysis in Part A, we could decide whether the vibration is present or absent by comparing the computed average energy in a PU with the pre-determined threshold λ_{fa}. λ_{fa} is partially determined by the false alarm probability P_{fa}. In real applications, FAR defined as the maximum number of false alarms tolerated by the user per unit time is more important than false alarm probability. The relationship between P_{fa} and FAR is as follows:

$$\begin{aligned} P_{fa} &= \frac{\text{Target FAR (for a given measurement period)}}{\text{number of PUs during that time}} \\ &= \frac{\text{Target FAR (for } t_N)}{floor\left(\frac{N}{N_s*(1-p)}\right) * M} \end{aligned} \tag{11}$$

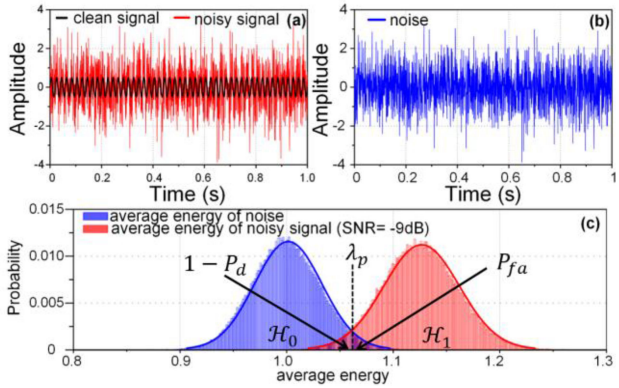

Fig. 4. (a) clean signal and noisy signal, (b) noise; average energy distributions of noise and noisy signal when $SNR = -9\,dB$.

For example, in the case that a DAS system has a 50 km FUT and 10 m spatial resolution (corresponding $M = 5 \times 10^3$), 2 kHz pulse repetition rate (corresponding $N = 1(day) * 24(hours) * 60(miniutes) * 60(seconds) * 2000(Hz) = 1.728 \times 10^8$), with only one false alarm per day, if we make a vibration detection every second with 50% overlap (corresponding $N_s = 2000$), then we have 8.64×10^8 PUs during one-day measurement period. According to (11), $P_{fa} = 1.157 \times 10^{-9}$. To keep FAR smaller than 1 FA/day, P_{fa} should be smaller than 1.157×10^{-9}. If noise power is known or can be estimated, λ_{fa} can be pre-determined according to (8).

C. Detection Probability With the Relationship of SNR, Processing Window Size, and False Alarm Probability

For a fix false alarm probability, detection probability is expected to be as high as possible. Replacing the definition of SNR in (3) and λ_{fa} in (8), we can get the following relationship:

$$P_d\ (\lambda_{fa}) = Q\left(\frac{Q^{-1}(P_{fa}) - SNR \cdot \sqrt{N_s/2}}{1+SNR}\right) \tag{12}$$

It indicates that with pre-determined P_{fa}, detection probability can be increased by improving SNR. To give an intuitive relationship between P_d and P_{fa}, a synthetic signal is demonstrated as shown in Fig. 4. Clean signal (black) in Fig. 4(a) shows a 40 Hz sine wave lasts one second period with 2 kHz sampling frequency. Gaussian white noise with a variance of one and zero mean as shown in Fig. 4(b) is added to the clean signal to get the noisy signal (red). SNR of the noisy signal is -9 dB. Then 10^5 times Monte Carlo simulations are conducted to calculate the average energy of noise and noisy signal according to (4). Average energy distributions are shown in Fig. 4(c). The overlap area shows the detection error probability, where the right-side area (under $\mathcal{H}_0$) of threshold λ_p denotes false alarm probability (P_{fa}) while the left-side area (under $\mathcal{H}_1$) denotes missed detection probability $(1 - P_d)$. Table II gives the threshold values under different false alarm probabilities when $N_s = 2000$, according to (8). For example, if $P_{fa} = 10^{-3}$ is required, we need to set the threshold to $\lambda_p = 1.0977 * \sigma_w^2$, according to Table II. However, it will lead to a detection probability, $P_d = 78.58\%$ when $SNR = -9dB$ according to (12). As can be seen in Fig. 4(c), lower false alarm probability can be achieved by increasing λ_p. However, higher λ_p will decrease detection probability.

TABLE II
λ_p FOR DIFFERENT FALSE ALARM PROBABILITIES WITH $N_s = 2000$

P_{fa}	10^{-3}	10^{-6}	10^{-9}	10^{-12}
λ_p	$1.0977*\sigma_w^2$	$1.1503*\sigma_w^2$	$1.1897*\sigma_w^2$	$1.2224*\sigma_w^2$

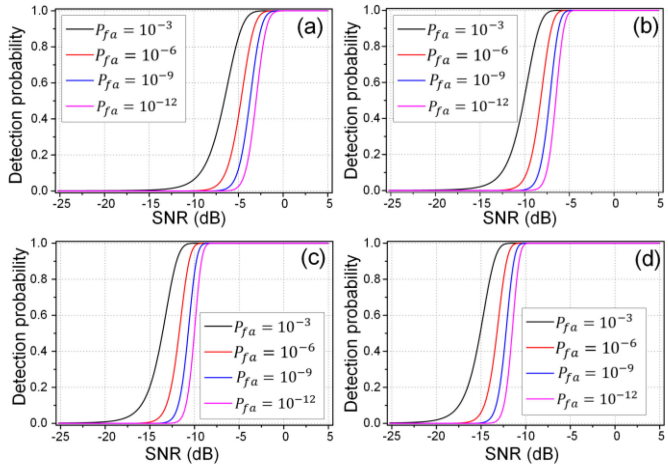

Fig. 5. Detection probabilities for different false alarm probabilities as SNR increases from -25 dB to 5 dB with N_s equals (a) 400, (b) 2000, (c) 10000, and (d) 20000.

Fig. 5 shows the detection probability as a function of SNR for different N_s and false alarm probabilities. We can see that under the same SNR and N_s, lower P_{fa} will lead to a lower detection probability before P_d reaches 100%. For example, in the case of $SNR = -5$ dB, $N_s = 400$, when P_{fa} is set to be 10^{-3}, $P_d = 85.31\%$. However, when P_{fa} is set as low as 10^{-12}, detection probability greatly reduced to $P_d = 2.58\%$. We can also observe that under the same P_{fa} and N_s, P_d increases as a function of SNR until P_d reaches 100%. The detection performance is also analyzed with respect to the processing window size N_s. It seems increasing N_s is a much simpler method to increases P_d compared with SNR improvement. However, SNR and N_s are highly correlated, in the case that the vibration lasts for a very short period but we set a large N_s, the calculated SNR during processing window N_s could be very low. Thus, the choice of N_s depends on the vibration to be detected. As an example, in perimeter intrusion detection, vibrations caused by people's walking last for a relatively long time, larger N_s can be selected. However, in some applications such as structural health monitoring, vibrations like crack may just last for a very short time, so a smaller N_s should be used.

D. Detection Performance With the Relationship of Noise

Ideally, average-energy-based method shows satisfactory performance as demonstrated in Fig. 5. 100% detection probability can be expected even in low SNR regimes. However, in practice, the true noise power is unknown and has to be estimated. The detection performance is highly susceptible to the accuracy of noise power estimation. Moreover, noise power always changes

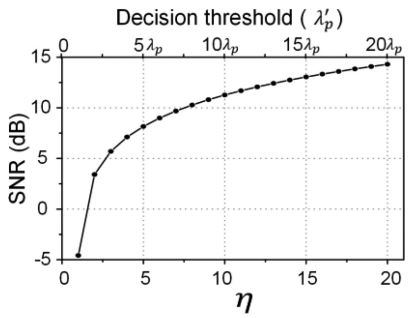

Fig. 6. Required decision threshold and SNR to achieve 100% detection probability and 10^{-9} false alarm probability for different noise uncertainty factor η, with $N_s = 2000$.

with time and position, which is referred to as 'noise uncertainty'. Dynamic noise power is denoted as $\widetilde{\sigma_w^2}$ and suppose it varies between $[\frac{1}{\eta}\sigma_w^2, \eta\sigma_w^2]$, where σ_w^2 is nominal noise power and $\eta \geq 1$ is noise uncertainty. Let us analyze two extreme cases:

1) If λ_p is calculated according to the lower bound $\frac{1}{\eta}\sigma_w^2$. For all the sensing events whose noise floor is significantly greater than $\frac{1}{\eta}\sigma_w^2$, the calculated average energy is higher than λ_p. In this case, the detector will declare the vibration present regardless of the true state of the vibration. This would result in a higher false alarm (FA) than expected.

2) If λ_p is calculated according to the upper bound $\eta\sigma_w^2$. For all the sensing events whose noise power is significantly lower than $\eta\sigma_w^2$, the calculated average energy is lower than λ_p. In this case, the detector will declare vibration absent, which will decrease the detection probability.

With the presence of noise uncertainty, the false alarm probability can be expressed as follows:

$$P_{fa}\ (\lambda) = \max\left[\ Q\left(\frac{\lambda-\widetilde{\sigma_w^2}}{\widetilde{\sigma_w^2}/\sqrt{N_s/2}}\right)\right]\ =\ Q\left(\frac{\lambda-\eta\sigma_w^2}{\eta\sigma_w^2/\sqrt{N_s/2}}\right) \tag{13}$$

Therefore, the decision threshold is η times the original one:

$$\lambda'_{fa} =\ \eta\sigma_w^2\ \left(1+\frac{Q^{-1}(P_{fa})}{\sqrt{N_s/2}}\right) = \eta\lambda_{fa} \tag{14}$$

The corresponding detection probability can be expressed as:

$$\begin{aligned} P_d\ \left(\lambda'_{fa}\right) &= \min\left[Q\left(\frac{\lambda'_{fa}-\left(\widetilde{\sigma_w^2}+\sigma_s^2\right)}{(\widetilde{\sigma_w^2}+\sigma_s^2)/\sqrt{N_s/2}}\right)\right] \\ &= Q\left(\frac{\lambda'_{fa}-\left(\frac{1}{\eta}\sigma_w^2+\sigma_s^2\right)}{(\frac{1}{\eta}\sigma_w^2+\sigma_s^2)/\sqrt{N_s/2}}\right) \end{aligned} \tag{15}$$

The required decision threshold and SNR to achieve 100% detection probability and 10^{-9} false alarm probability for different noise uncertainty factor when $N_s = 2000$ is shown in Fig. 6. We can see that much higher decision threshold and SNR are required to achieve the target P_{fa} and P_d compared with the case that noise power is static, i.e., $\eta = 1$.

IV. Autocorrelation-Energy Based Method

To solve the problem of noise uncertainty in average-energy-based method, we propose a noise-irrelevant threshold setting method based on the autocorrelation energy.

A. Characteristics of Autocorrelation

As discussed above, a noisy signal can be expressed as $x\,(n) = s(n) + w(n)\ 0 \leq n \leq N_s - 1$. If the noise is uncorrelated with the signal, the autocorrelation coefficient (ACC) of a noisy signal is the sum of ACC of the clean signal and noise:

$$\begin{aligned} c_{xx}\ (n) &= E\left[x\,(i)\,x\,(i-n)\right] \\ &= E\left[\{s\,(i)+w\,(i)\}\,\{s\,(i-n)+w\,(i-n)\}\right] \\ &= c_{ss}\ (n)+c_{sw}\,(n)+c_{ws}\,(n)+c_{ww}\,(n) \\ &= c_{ss}\ (n)+c_{ww}\,(n) \end{aligned} \tag{16}$$

Typically, noise $w(n)$ is statistically independent of signal $s(n)$. The cross-correlation terms $c_{sw}(n)$ and $c_{ws}(n)$ are both zero since $E\left[w(n)\right] = 0$, so as the ACC of white noise:

$$\begin{aligned} c_{ww}\ (n) &= E\left[w\,(i)\,w\,(i-n)\right] \\ &= E\left[w\,(i)\right]E\left[w\,(i-n)\right] \\ &= 0\ n \neq 0 \end{aligned} \tag{17}$$

Since the samples of white noise are statistically independent with zero mean, ACC of white noise is 0 when $n \neq 0$. When $n = 0, c_{ww}\,(n) = \sigma_w^2$. Thus, ACC of a zero-mean white noise can be expressed as: $c_{ww}(n) \approx \sigma_w^2\ \delta(n),\ 0 \leq n \leq N_s - 1$. As the value of N_s increases, the approximation becomes more accurate. When $n > 0, c_{ww}(n) \approx 0$. Therefore, ACC of a noisy signal $x(n)$ can be simplified to:

$$c_{xx}\,(n) \approx c_{ss}\,(n) + \sigma_w^2\ \delta\,(n) \tag{18}$$

For $n > 0$, we have $c_{xx}(n) \approx c_{ss}(n)$, which means ACC is robust to noise.

B. Theoretical Model

The steps of the proposed autocorrelation-energy based method are given as follows:

1) Short-time average energy is computed, $\mu = \frac{1}{N_s}\sum_{n=0}^{N_s-1} x(n)^2$.
2) Sum of first K absolute ACC is calculated, $\rho = \sum_{n=0}^{K-1}\left|c_{xx}(n)\right|$.
3) A decision on the presence of vibration is made by comparing the ratio ρ/μ with a threshold.

First, let us express ρ under $\mathcal{H}_0$ and $\mathcal{H}_1$ as follows:

$$\begin{aligned} \rho\ &= \sum_{n=0}^{K-1}\left|c_{xx}\,(n)\right| \\ &= \begin{cases} \sigma_w^2\ +\sum_{n=1}^{K-1}\left|c_{ww}\,(n)\right| & under\ \mathcal{H}_0 \\ \sigma_w^2+\sigma_s^2+\sum_{n=1}^{K-1}\left|c_{ss}\,(n)\right| & under\ \ \mathcal{H}_1 \end{cases} \end{aligned} \tag{19}$$

When N_s is large enough, ρ is approximate with Gaussian distribution. Under $\mathcal{H}_0$, the expected value of ρ is [24]:

$$E\ [\rho] = E\left[|c_{ww}(0)|\right] + E\left[|c_{ww}(k>0)|\right] = \left[1+(K-1)\sqrt{2/\pi N_s}\right]\sigma_w^2 \tag{20}$$

Therefore, ρ/μ under $\mathcal{H}_0$ can be expressed as:

$$\frac{\rho}{\mu} \approx \frac{E[\rho]}{E[\mu]} = \frac{\left[1+(K-1)\sqrt{2/\pi N_s}\right]\sigma_w^2}{\sigma_w^2} = \left[1+(K-1)\sqrt{2/\pi N_s}\right] \tag{21}$$

The false alarm probability is:

$$P_{fa}\ (\lambda) = P\left(\frac{\rho}{\mu} > \lambda\ \mathcal{H}_0\right)$$

$$\approx \mathrm{P}\left(\frac{\mu-\sigma_w^2}{\sqrt{2/N_s}\sigma_w^2} < \frac{\frac{1}{\lambda_p}\left[1+(K-1)\sqrt{2/\pi N_s}\right]\sigma_w^2 - \sigma_w^2}{\sqrt{2/N_s}\sigma_w^2}\ \mathcal{H}_0\right)$$

$$= 1 - Q\left(\frac{\frac{1}{\lambda}\left[1+(K-1)\sqrt{2/\pi N_s}\right]-1}{\sqrt{2/N_s}}\right) \tag{22}$$

For a given P_{fa}, the threshold is:

$$\lambda_p = \frac{1+(K-1)\sqrt{2/\pi N_s}}{1-\sqrt{2/N_s}Q^{-1}(P_{fa})} \tag{23}$$

We can see that the threshold determination equation in the autocorrelation-energy-based method is not related to the noise anymore.

Under $\mathcal{H}_1$, the expected value of ρ is:

$$E\ [\rho] = E\left[|c_{xx}(0)|\right] + E\left[|c_{xx}(n>0)|\right] = \sigma_w^2 + \sigma_s^2 + \sum_{n=1}^{K-1}|\alpha_n|\,\sigma_s^2 \tag{24}$$

where $|\alpha_n| = E[s(i)s(i-n)]/\sigma_s^2 \quad (0 \le |\alpha_n| \le 1)$is the normalized correlation among signal samples. We denote $\Upsilon = \sum_{n=1}^{K-1}|\alpha_n|$, which represents the correlation strength among consecutive K samples. The ρ/μ ratio under $\mathcal{H}_1$ can be expressed as:

$$\frac{\rho}{\mu} \approx \frac{E[\rho]}{E[\mu]} = \frac{\sigma_w^2+\sigma_s^2+\Upsilon\sigma_s^2}{\sigma_w^2+\sigma_s^2} = 1+\frac{\Upsilon * SNR}{SNR+1} \tag{25}$$

The detection probability is:

$$P_d\ (\lambda_p) = P\left(\frac{\rho}{\mu} > \lambda_p\ \mathcal{H}_1\right)$$

$$\approx P\left(\frac{\mu-(\sigma_w^2+\sigma_s^2)}{\sqrt{2/N_s}(\sigma_w^2+\sigma_s^2)} < \frac{\frac{1}{\lambda_p}\left[1+\frac{\Upsilon * SNR}{SNR+1}\right](\sigma_w^2+\sigma_s^2)-(\sigma_w^2+\sigma_s^2)}{\sqrt{2/N_s}(\sigma_w^2+\sigma_s^2)}\ \mathcal{H}_1\right)$$

$$= 1 - Q\left(\frac{\frac{1}{\lambda_p}\left[1+\frac{\Upsilon * SNR}{SNR+1}\right]-1}{\sqrt{2/N_s}}\right) \tag{26}$$

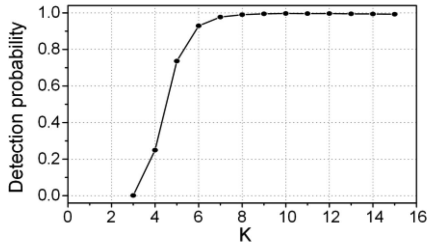

Fig. 7. Detection probability with different K.

TABLE III
λ_p FOR DIFFERENT FALSE ALARM PROBABILITIES WITH $N_s = 2000$, $K = 10$

P_{fa}	10^{-3}	10^{-6}	10^{-9}	10^{-12}
λ_p	1.2863	1.3659	1.4322	1.4926

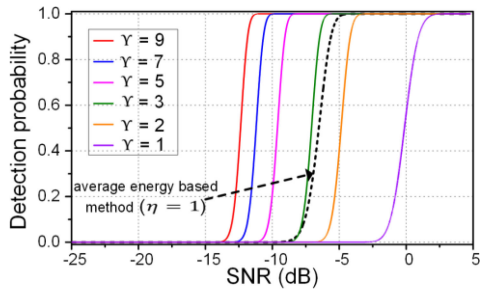

Fig. 8. Detection probabilities with different correlation strengths when SNR increases from −25 dB to 5 dB, with $P_{fa} = 10^{-9}$ and $N_s = 2000$.

C. Detection Probability With the Relationship of K, Υ, and SNR

- ACC summation number K: according to (23), the decision threshold is related to the number of K. To explore the impact of K, we use the same sine wave in Fig. 4(a) and fix $SNR = -9dB$ and $P_{fa} = 10^{-5}$. 10^5 times Monte Carlo simulations are performed to calculate detection probability for different K. The result is shown in Fig. 7. We can see that with K > 8 the detection probability is not very sensitive to K. Therefore, we fix $K = 10$ in the following work. Table III gives threshold values for different false alarm probabilities with $N_s = 2000$ and $K = 10$.
- Signal correlation strength Υ and SNR: according to (26), the detection probability is Υ related, where $\Upsilon = \sum_{n=1}^{K-1}|\alpha_n|\,.\,\alpha_n$ is the normalized correlation among signal samples with n delay, and it reflects the randomness of a signal. For a random signal such as white noise, α_n is near zero for $n > 0$; for non-random signal, one or more α_k will be significantly non-zero when $n > 0$. With $K = 10$ and $0 \le |\alpha_n| \le 1$, Υ is restricted to $[0, 9]$. If P_{fa} is fixed at 10^{-9} and N_s is fixed at 2000, detection probabilities with different Υ under various SNR are calculated and shown in Fig. 8. The dashed line is the performance of average-energy-based method assuming that the noise power is perfectly estimated, i.e., $\eta = 1$. The results indicate that when $\Upsilon \ge 3$, autocorrelation-energy-based method offers better performance than average-energy-based method.

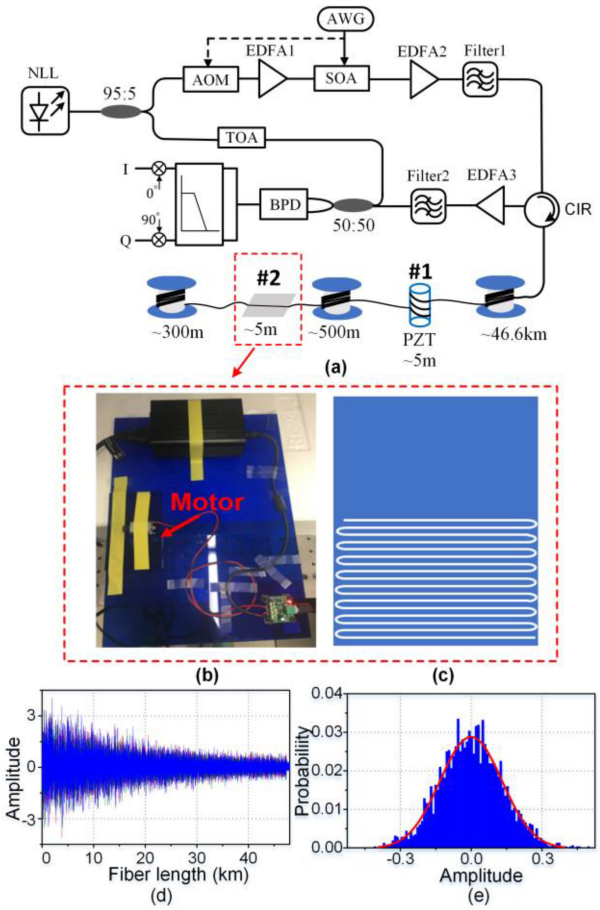

Fig. 9. (a) Experimental setup of DAS; (b) vibration source #2 with a motor fixed on a semi-suspended plastic sheet, 5m-long fiber section is fixed on the backside of the plastic sheet as (c); (d) Differential RBS traces along the FUT; (e) signal amplitude distribution of 2000 scans at position 46km. AWG: arbitrary waveform generator; EDFA: erbium-doped fiber amplifier; TOA: tunable optical attenuator; CIR: circulator; BPD: balanced photo-detector; PZT: piezoelectric transducer.

However, when $\Upsilon < 3$, detection probability will be degraded. Therefore, to detect weakly correlated vibration signal, higher SNR is needed.

V. Experimental Results and Discussions

A. Experimental Setup of DAS

The experimental setup of the DAS system based on heterodyne detection is shown in Fig. 9. A narrow-linewidth laser (NLL, NKT Photonics X15) with 100 Hz frequency width at 1550.12 nm is used as the optical source. The output of NLL is split into two branches with a 95:5 coupler. In the upper branch, the continuous wave (CW) is firstly modulated by an acoustic optical modulator (AOM) with an 80 MHz frequency shift. The AOM is cascaded with a semiconductor optical amplifier (SOA, INPHENIX: IPSAD1501) to increase the extinction ratio (ER). In order to synchronize the AOM and the SOA, the pulse delay is properly adjusted through the arbitrary waveform generator (AWG). Two erbium-doped fiber amplifiers (EDFA1 and EDFA2) are used to boost the optical pulse power. The amplified spontaneous emission (ASE) noise is filtered out by an optical bandpass filter with 0.8 nm width. Then the optical pulses are launched into the FUT. The RBSs are further amplified by EDFA3 and followed by another 0.8 nm bandpass optical filter. Then it is combined with the optical local oscillator in the lower branch and launched into a balanced photo-detector (BPD). The data are collected by an 8-bit data acquisition system with a sampling rate of 625 MS/s. After in-phase/quadrature (I/Q) demodulation, both amplitude and phase information can be obtained. In the following work, vibration detection is based on the demodulated amplitude. It should be mentioned that the demodulated amplitude in the coherent detection DAS conveys the same information as the direct detection DAS, therefore, the proposed method is also suitable for the direct detection DAS system.To reduce data size, the data are downsampled by a factor of 20 along the fast-time axis after I/Q demodulation.

In our experiment, the FUT is G652 single-mode fiber (SMF) and the total length is around 47.4 km. The pulse repetition rate is set to 2 kHz and the pulse width is 50ns. A piezoelectric transducer (PZT) cylinder with 5 m fiber wrapped is put at the position around 46.6 km to generate the first vibration. The PZT is driven by a 100 Hz square wave. At the position around 47.1 km, a motor works on a semi-suspended plastic sheet to generate the second vibration as shown in Fig. 9(b). A 5 m-long fiber section is pulled tightly and fixed with glue on the backside of the plastic sheet as shown in Fig. 9(c). When the mechanical waves caused by the motor propagate to the plastic sheet, it will induce deformations of the fiber on it. The experiment is carried out in an open environment, so the FUT is subjected to both DAS system noise and environmental noise.

Several differential RBS traces along the FUT is shown in Fig. 9(d). At position 46 km, signal amplitude distribution of 2000 scans is shown in Fig. 9(e), which is Gaussian distributed. To detect the vibrations along the FUT, the RBS traces are processed every second with a 0.5-second overlap along slow-time axis for every position on the FUT. In total, we have 1.07×10^8 PUs within a one-hour measurement period. If we set target FAR to 1/hour, then corresponding P_{fa} is 9.35×10^{-9}. In the following work, measured FA is defined as the total number of false alarms and measured false alarm probability is calculated by $P_{fa}^M = \frac{measured\ FA}{total\ number\ of\ PU}$. Detection probability of vibration #1 or #2 is calculated by $P_{d1\ or\ d2} = \frac{number\ of\ detected\ vibration\ \#1\ or\ \#2}{number\ of\ PU\ at\ position\ \#1\ or\ \#2}$.

B. Average-Energy-Based Method for Vibration Detection

The detection performance of average-energy-based method is analyzed first. The calculated average energy along the FUT is shown in Fig. 10. Zoom-in view of the last 2.4 km is shown in the inset. According to (8), the threshold is estimated as the noise power multiplied by 1.1778. The acquired 10 minutes RBS traces without applying any vibration are used to estimate the noise power for threshold determination. With the existence of noise uncertainty, the estimated noise power is set to the upper bound of the noise power to achieve target FAR. Therefore, the estimated noise power at each position is set to the maximum power. The threshold is shown in Fig. 10 with a blackline (λ_p). Using λ_p as a decision threshold, the detection performance

TABLE IV
DETECTION PERFORMANCE COMPARISON OF AVERAGE-ENERGY-BASED METHOD AND AUTOCORRELATION-ENERGY-BASED METHOD

Method \ Detection performance	Decision threshold λ_p				Processing time per second along FUT
	$P_{d1}(\#1)$	$P_{d2}(\#2)$	Measured FA	P_{fa}^{M}	
Average-energy-based method	63%	96.6%	9384	8.77×10^{-5}	0.14 ms
Autocorrelation-energy-based method	100%	98.1%	12	1.12×10^{-7}	111.67 ms

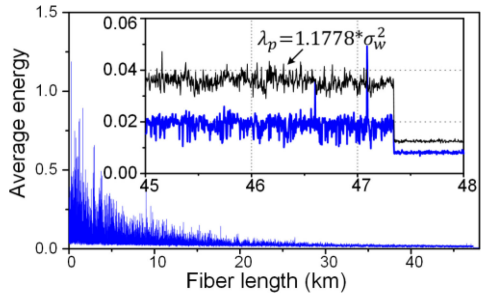

Fig. 10. Average energy along the FUT. Blackline represents the decision threshold.

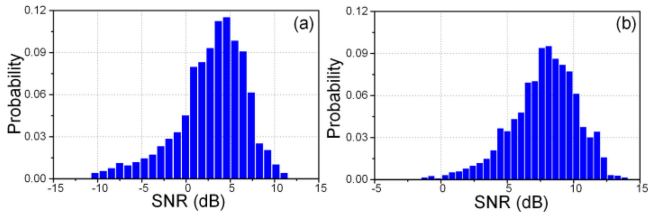

Fig. 11. SNR distribution of (a) vibration #1, and (b) vibration #2.

is shown in Table IV. The detection probability is 58.6% for vibration #1 and 81.8% for vibration #2. The detection probability of vibration #2 is higher than vibration #1 since vibration #2 has a higher overall SNR, as shown in Fig. 14. The SNR is estimated by: $\widetilde{SNR} = (P_{vib} - \overline{P_{non-vib}})/\overline{P_{non-vib}}$, where P_{vib} is the power of vibration, and $\overline{P_{non-vib}}$ is the mean power of the 200 m section in front of vibration positions. During a one-hour measurement period, the SNR of vibration #1 varies from -10.3 dB to 11.1 dB with an average of 2.5 dB and that varies from -2.2 dB to 13.8 dB with an average of 7.7 dB for vibration $\#2$. Fig. 11 shows that SNR is not a constant but instead fluctuates in a wide range due to signal fading phenomena and time-varying signals and noise.

During a one-hour measurement period, the total number of FA is 9384 and corresponds to 8.77×10^{-5} measured false alarm probability. To reduce the false alarm probability, we need to set a higher decision threshold, however, this will decrease the detection probability. A possible solution to mitigate the effect of noise uncertainty is adapting the decision threshold to the noise power at different positions and different time slots. For this, we need to estimate the noise power in real-time. Noise estimation algorithms in [25], [26] can be used to assist the determination of a dynamic decision threshold at the cost of higher computational complexity. Another proposal to improve the detection performance is to reduce noise uncertainty in DAS. Noise uncertainty caused by signal fading can be alleviated by

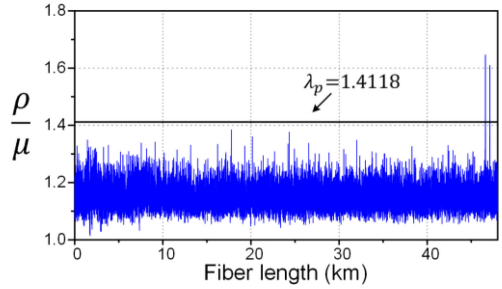

Fig. 12. ρ/μ along the FUT. Blackline represents the decision threshold λ_p.

schemes in [9], [10] for hardware optimization and can also be reduced by denoising algorithms such as in [6], [11], [13].

C. Autocorrelation-Energy-Based Method for Vibration Detection

For the average-energy-based method, the knowledge of accurate noise power is essential in threshold determination. Inaccurate estimated noise power will result in detection performance degradation. However, in most situations, it is difficult to pre-estimate the noise power. Then we use autocorrelation-energy-based method for vibration detection without knowing the noise power information. With the same data in Fig. 10, ρ/μ along the FUT is shown in Fig. 12. Unlike average energy along the FUT that decreases exponentially, ρ/μ at different positions are at the same level with a confined fluctuation range and the mean of ρ/μ is determined by (21). Therefore, a single threshold can be applied for vibration detection at different positions. According to (23), the decision threshold value is 1.4118 when the target FAR is 1FA/hour, which is shown in Fig. 12 with blackline (λ_p). The detection probabilities are 100% for vibration #1 and 98.6% for vibration #2, as shown in Table IV. Using λ_p as decision threshold, measured FA is 12 within one hour, corresponding to 1.12×10^{-7} false alarm probability, which is two orders of magnitude smaller than average-energy-based method.

As shown in Fig. 13, ρ/μ of noise distribution is on the left side while that of vibrations is on the right side and they are well separated. Ideally, if the non-vibration positions along the FUT are all white noise, ρ/μ distribution of non-vibration positions follows a perfectly symmetric Gaussian distribution. However, as shown in Fig. 13, ρ/μ of noise is slightly right-skewed, which may due to the non-white environmental noise. Vibration #1 has a higher overall ρ/μ, which brings a higher detection probability. ρ/μ is related with both SNR and correlation strength. Estimated SNR distributions of vibration #1 and #2 are shown in Fig.11. To estimate the correlation strength of two different vibrations, their phases are unwrapped. Demodulated phases of vibration #1 and #2 and their corresponding power spectral density (PSD)

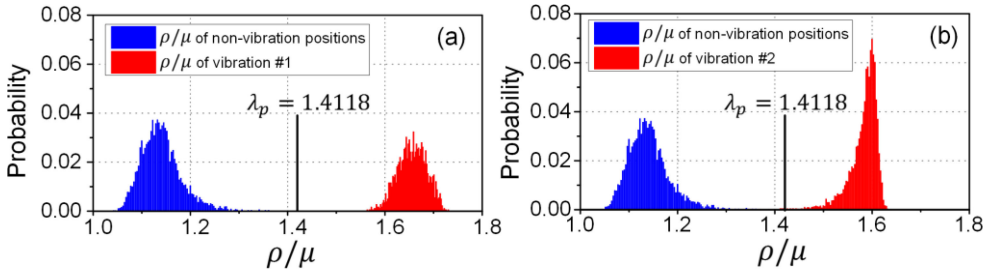

Fig. 13. ρ/μ distributions of non-vibration positions and (a) vibration #1, and (b) vibration #2.

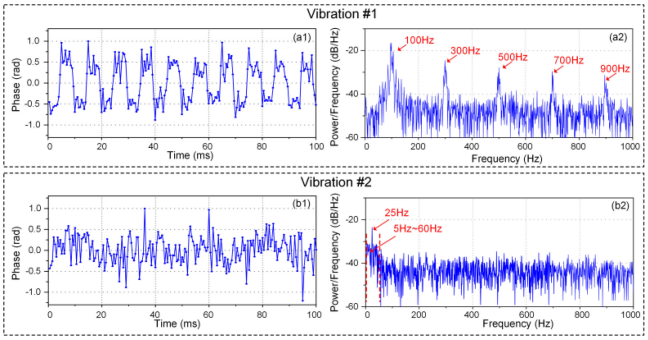

Fig. 14. Demodulated phasae of (a1) vibration #1, (b1) vibration #2. Power spectral density of (a2) vibration #1, (b2) vibration #2.

are shown in Fig. 14. Vibration #1 is a square wave and presents a strong repeating pattern as shown in Fig. 14(a1). The estimated correlation strength $\tilde{\Upsilon}_{\#1} = 6.2$. Vibration #2 caused by mechanical vibrations does not show a notable pattern, as shown in Fig. 14 (a2). From its PSD, we can see that it has a weak periodicity at 25 Hz and has a narrow frequency band from 5 Hz to 60 Hz. The estimated correlation strength $\tilde{\Upsilon}_{\#2} = 2.17$. $\tilde{\Upsilon}_{\#1}$ is much higher than $\tilde{\Upsilon}_{\#2}$ and it can explain why vibration #2 has a higher detection probability than vibration #1 even though it has a lower overall SNR.

The data processing time of the two methods are also computed, as shown in Table IV. The processing time per second along the FUT is 0.14 ms for average-energy-based method and 116.67 ms for autocorrelation-energy-based method. The two algorithms are both implemented using Matlab offline with AMD Ryzen7 2700X Eight-Core CPU and 32G RAMs. The processing time for the autocorrelation-energy-based method is about 800 times slower than the average-energy-based method, but it is still fast enough and can be used for real-time monitoring.

D. Discussions

- For decision threshold: A threshold λ_p is required to decide whether the vibration is present or absent. This threshold determines both P_d and P_{fa}. A common strategy for setting λ_p is based on a target FAR and can be obtained by inverting the analytical expression of P_{fa}. For the average-energy-based method, the decision threshold is a function of P_{fa} and noise power, as indicated by (8). The actual noise power is generally unknown in DAS and getting accurate knowledge of noise power is extremely difficult since the noise power changes temporally and spatially. We can use the upper bound of noise power in threshold calculation as given in (14), which requires a long time to record the background noise. And setting decision threshold based on the historic background noise may not reliable for current data. Instead, a better choice is to use the autocorrelation-energy-based method, with which the decision threshold is immune to noise uncertainty and only determined by P_{fa} according to (23).
- For environmental noise induced FA: background noise consists of DAS system noise and environmental noise. The DAS system noise can be regarded as additional white Gaussian noise (AWGN) in a short time period. The environmental noises from wind interference, structure-free vibration and the temperature change may not be AWGN and will interfere with the vibration signal. Therefore, environmental noises may cause additional false alarms and they cannot be eliminated by just increasing the decision threshold level in the vibration detection stage. As an alternative, they can be ruled out in the pattern recognition stage based on some prior knowledge about the vibration signal.

VI. Conclusion

In this work, we propose the autocorrelation-energy-based method for vibration detection and compare it with the average-energy-based method in a DAS system. Statistical theories have been used for guiding the decision threshold setting and quantifying the relationship between detection performance and the SNR. The experiment is carried out to evaluate the detection performance of two methods. It is shown that the proposed autocorrelation-energy-based method gives better detection performance compared with the average-energy-based method. Furthermore, if the vibration signal is highly correlated, detection probability will be enhanced. The proposed method does not need any prior knowledge to detect vibrations and does not rely on the noise power to set the decision threshold, which makes it useful for vibration detection in DAS.

Appendix

Lemma1: Sum of squares of $\boldsymbol{N_s}$ independent standard Gaussian random variables is a Chi-square random variable with $\boldsymbol{N_s}$ degrees of freedom.

Let $N_s \in \mathbb{N}$. We say X has a Chi-square distribution with N_s degrees of freedom ($\chi^2_{N_s}$) if and only if its probability density function (PDF) is:

$$f_\chi\ (x, N_s) = \begin{cases} \frac{1}{2^{N_s/2}\Gamma(N_s/2)} x^{N_s/2-1} e^{-x/2}\ x \geq 0 \\ 0\ x < 0 \end{cases}$$

where $\Gamma(\cdot)$ denotes Gamma function. We denote $c = \frac{1}{2^{N_s/2}\Gamma(N_s/2)}$.

Proof A1: the square of a standard Gaussian random variable is a Chi-square random variable with 1 degree of freedom.

Let Z be a standard Gaussian random variable and let X be its square: $X = Z^2$.

- For $x \geq 0$, the distribution of X is:

$$F_X\ (x) = P\ (X \leq x) = P\ \left(Z^2 \leq x\right) = \int_{-x^{\frac{1}{2}}}^{x^{\frac{1}{2}}} f_z\,(z)\,dz$$

where $f_z(z)$ is the probability density function of a standard Gaussian random variable: $f_z\ (z) = \frac{1}{\sqrt{2\pi}} \exp(-\frac{1}{2}z^2)$

- For $x < 0$, $F_X\ (x) = 0$. Because $X = Z^2$, it will not be negative.

Using Leibniz integral rule and the fact that density function is the derivative of the distribution function, the PDF of X, denoted by $f_X(x)$, is obtained as follows:

- For $x \geq 0$:

$$\begin{aligned} f_X\ (x) &= \frac{dF_X\,(x)}{dx} \\ &= f_z\ \left(x^{\frac{1}{2}}\right) \frac{d\left(x^{\frac{1}{2}}\right)}{dx} - f_z\left(-x^{\frac{1}{2}}\right)\ \frac{d\left(-x^{\frac{1}{2}}\right)}{dx} \\ &= \frac{1}{\sqrt{2\pi}}\ x^{-\frac{1}{2}}\ \exp\left(-\frac{1}{2}x\right) \\ &= \frac{1}{2^{\frac{1}{2}}\Gamma\left(\frac{1}{2}\right)} x^{\frac{1}{2}-1} \exp\left(-\frac{1}{2}x\right) \end{aligned}$$

- For $x < 0$, trivially, $f_X\ (x) = 0$.

Therefore, $f_X(x)$ is the PDF of a Chi-square random variable with 1 degree of freedom.

$$f_X\ (x) = \begin{cases} \frac{1}{2^{1/2}\Gamma(1/2)} x^{1/2-1} e^{-1/2}\ x \geq 0 \\ 0\ x < 0 \end{cases}$$

Proof A2: sum of N_s independent Chi-square random variables is a Chi-square random variable with N_s degrees of freedom.

The distribution of a random variable is often characterized in terms of its moment generating function. The moment generating function of a Chi-square random variable X with 1 degree of freedom is:

$$\begin{aligned} &M_X\ (t) = E\left[\exp\left(tX\right)\right] \\ &= c\int_0^\infty \exp\left(tx\right) x^{\frac{1}{2}-1} \exp\left(-\frac{1}{2}x\right) \\ &dx = c\int_0^\infty x^{\frac{1}{2}-1} \exp\left(-\left(\frac{1}{2}-t\right)x\right) \\ &dx\ \left\{let\ y\ = \left(\frac{1}{2}-t\right)\ x\right\} \\ &= c\left(\frac{2}{1-2t}\right)^{\frac{1}{2}} \int_0^\infty \mathrm{y}^{\frac{1}{2}-1} \exp\left(-y\right) \\ &dy = \frac{1}{2^{\frac{1}{2}}\Gamma\left(\frac{1}{2}\right)} \left(\frac{2}{1-2t}\right)^{\frac{1}{2}} \Gamma\left(\frac{1}{2}\right) = (1-2t)^{-1/2} \end{aligned}$$

The moment generating function of a sum of mutually independent random variables is just the product of their moment generating functions. Therefore, sum of N_s independent Chi-square random variables is:

$$M_X\ (t) = \prod_{i=1}^{N_s} M_{X_i(t)}\ = \prod_{i=1}^{N_s} (1-2t)^{-1/2}\ = (1-2t)^{-N_s/2}$$

The result shows that moment generating function of X is the moment generating function of a Chi-square random variable with N_s degree of freedom. Therefore, X is a Chi-square random variable with N_s degrees of freedom, $X \sim \chi^2_{N_s}$.

Lemma2: The expected value of a Chi-square random variable with N_s degrees of freedom is $E\ (X) = N_s$, the variance is $Var\ (X) = 2N_s$.

The expected value of a Chi-square random variable with N_s degree of freedom is:

$$\begin{aligned} &E\ (X) = \int_0^\infty x f_\chi\,(x, N_s)\,dx\ = c\int_0^\infty x^{N_s/2+1} e^{-\frac{x}{2}} dx \\ &= c\left\{-x^{N_s/2} e^{-x/2}|_0^\infty + \int_0^\infty N x^{N_s/2-1} e^{-x/2} dx\right\} \\ &= N_s \int_0^\infty f_\chi\,(x, N_s)\,dx\ = N_s \\ &E\ \left[X^2\right] = \int_0^\infty x^2 f_\chi\,(x, N_s)\,dx\ = c\int_0^\infty x^{N_s/2+1} e^{-\frac{x}{2}}\ dx \\ &= c\ \left\{-2x^{N_s/2+1} e^{-x/2}|_0^\infty + \int_0^\infty N_s x^{N_s/2-1} e^{-\frac{x}{2}}\ dx\right\} \\ &= N_s\ (N_s+2) \end{aligned}$$

Therefore, the variance of a Chi-square random variable with N_s degree of freedom is:

$$Var\ (X) = E\left[X^2\right] - E[X]^2 = N_s\ (N_s+2) - {N_s}^2 = 2N_s$$

Under $\mathcal{H}_0$, we have:

$$E\ (f_u\,(x)) = E\left(\frac{\sigma_w^2}{N_s} f_\chi\left(\frac{x\sigma_w^2}{N_s}, N_s\right)\right) = \frac{\sigma_w^2}{N_s}\ \cdot N_s = \sigma_w^2$$

$$Var\ (f_u\,(x)) = Var\left(\frac{\sigma_w^2}{N_s} f_\chi\left(\frac{x\sigma_w^2}{N_s}, N_s\right)\right)$$

$$= \frac{\sigma_w^4}{N^2}\ \cdot 2\,N_s = \frac{2\sigma_w^4}{N_s}$$

Under $\mathcal{H}_1$, we have:

$$E\ (f_u\,(x)) = E\left(\frac{\sigma_w^2\ +\sigma_s^2}{N_s} f_\chi\left(\frac{x(\sigma_w^2\ +\sigma_s^2)}{N_s}, N_s\right)\right)$$

$$= \frac{\sigma_w^2\ +\sigma_s^2}{N_s}\ \cdot N_s$$

$$= \sigma_w^2\ \ +\sigma_s^2$$

$$Var\ (f_u\,(x)) = Var\left(\frac{\sigma_w^2+\sigma_s^2}{N_s} f_\chi\left(\frac{x(\sigma_w^2\ +\sigma_s^2)}{N_s}, N_s\right)\right)$$

$$= \left(\frac{\sigma_n^2\ +\sigma_s^2}{N_s}\right)^2\ \cdot 2N_s$$

$$= \frac{2\left(\sigma_w^2\ +\sigma_s^2\right)^2}{N_s}$$

REFERENCES

[1] S. Dou *et al.*, "Distributed acoustic sensing for seismic monitoring of the near surface: A traffic-noise interferometry case study," *Sci. Rep.*, vol. 7, no. 1, pp. 1–12, 2017.

[2] J. C. Juarez, E. W. Maier, K. N. Choi, and H. F. Taylor, "Distributed fiber-optic intrusion sensor system," *J. Lightw. Technol.*, vol. 23, no. 6, pp. 2081–2087, Jun. 2005.

[3] F. Tanimola and D. Hill, "Distributed fiber optic sensors for pipeline protection," *J. Natural Gas Sci. Eng.*, vol. 1, nos. 4/5, pp. 134–143, 2009.

[4] P. Healey, "Fading in heterodyne OTDR," *Electron. Lett.*, vol. 20, no. 1, pp. 30–32, 1984.

[5] H. F. Taylor and C. E. Lee, "Apparatus and method for fiber optic intrusion sensing," U.S. Patent 5194847A, Mar. 1993.

[6] Y. Lu, T. Zhu, L. Chen, and X. Bao, "Distributed vibration sensor based on coherent detection of phase-OTDR," *J. Lightw. Technol.*, vol. 28, no. 22, pp. 3243–3249, Nov. 2010.

[7] H. F. Martins, S. Martin-Lopez, P. Corredera, M. L. Filograno, O. Frazao, and M. Gonzalez-Herraez, "Phase-sensitive optical time domain reflectometer assisted by first-order raman amplification for distributed vibration sensing over >100 km," *J. Lightw. Technol.*, vol. 32, no. 8, pp. 1510–1518, Apr. 2014.

[8] Z. N. Wang *et al.*, "Ultra-long phase-sensitive OTDR with hybrid distributed amplification," *Opt. Lett.*, vol. 39, no. 20, pp. 5866–5869, 2014.

[9] M. Ren, P. Lu, L. Chen, and X. Bao, "Theoretical and experimental analysis of φ-OTDR based on polarization diversity detection," *IEEE Photon. Lett.*, vol. 28, no. 6, pp. 697–700, Mar. 2016.

[10] A. H. Hartog *et al.*, "The use of multi-frequency acquisition to significantly improve the quality of fibre-optic-distributed vibration sensing," *Geophy. Prospecting*, vol. 66, pp. 192–202, 2018.

[11] Z. Qin, L. Chen, and X. Bao, "Wavelet denoising method for improving detection performance of distributed vibration sensor," *IEEE Photon. Technol. Lett.*, vol. 24, no. 7, pp. 542–544, Apr. 2012.

[12] T. Zhu, X. Xiao, Q. He, and D. Diao, "Enhancement of SNR and spatial resolution in φ-OTDR system by using 2-D edge detection method," *J. Lightw. Technol.*, vol. 31, no. 17, pp. 2851–2856, Sep. 2013.

[13] H. He *et al.*, "SNR enhancement in phase-sensitive OTDR with adaptive 2-D bilateral filtering algorithm," *IEEE Photon. J.*, vol. 9, no. 3, pp. 1–10, Jun. 2017.

[14] H. Zhu. C. Pan, and X. Sun, "Vibration pattern recognition and classification in OTDR based distributed optical-fiber vibration sensing system," in *Proc. SPIE*, San Diego, CA, United States, 2014, Art. no. 9062.

[15] F. Jiang, H. Li, Z. Zhang, Y. Zhang, and X. Zhang, "Localization and discrimination of the perturbation signals in fiber distributed acoustic sensing systems using spatial average kurtosis," *Sensors*, vol. 18, no. 9, 2018, Art. no. 2839.

[16] S. Liang, X. Sheng, and S. Lou, "Experimental investigation on lower nuisance alarm rate phase-sensitive OTDR using the combination of a Mach–Zehnder interferometer," *Phys. Technol.*, vol. 75, pp. 117–123, 2016.

[17] B. M. Tabi Fouda, D. Han, B. An, X. Lu, and Q. Tian, "Events detection and recognition by the fiber vibration system based on power spectrum estimation," *Adv. Mech. Eng.*, vol. 10, no. 11, 2018, Art. no. 1687814018808679.

[18] J. Tejedor *et al.*, "Real field deployment of a smart fiber-optic surveillance system for pipeline integrity threat detection: Architectural issues and blind field test results," *J. Lightw. Technol.*, vol. 36, no. 4, pp. 1052–1062, Feb. 2018.

[19] H. Urkowitz, "Energy detection of unkown deterministic signals," *Proc. IEEE*, vol. 55, no. 4, pp. 523–531, Apr. 1967.

[20] J. Zhou, Z. Pan, Q. Ye, H. Cai, R. Qu, and Z. Fang, "Characteristics and explanations of interference fading of a φ-OTDR with a multi-frequency source," *J. Lightw. Technol.*, vol. 31, no. 17, pp. 2947–2954, Sep. 2013.

[21] J. Tejedor, J. Macias-Guarasa, H. F. Martins, J. Pastor-Graells, P. Corredera, and S. Martin-Lopez, "Machine learning methods for pipeline surveillance systems based on distributed acoustic sensing: A review," *Appl. Sci.*, vol. 7, no. 8, pp. 841, 2017.

[22] M. Adeel *et al.*, "Impact-Based feature extraction utilizing differential signals of phase-sensitive OTDR," *J. Lightw. Technol.*, vol. 38, no. 8, pp. 2539–2546, Apr. 2020.

[23] M. Rosenblatt, "A central limit theorem and a strong mixing condition," in *Proc. Nat. Acad. Sci.*, vol. 42, no. 1, pp. 43–47, Jan. 1956.

[24] Y. Zeng and Y. C. Liang, "Spectrum-sensing algorithms for cognitive radio based on statistical covariances," " *IEEE Trans. Veh. Technol.*, vol. 58, no. 4, pp. 1804–1815, May 2008.

[25] R. Martin, "Noise power spectral density estimation based on optimal smoothing and minimum statistics," *IEEE Trans. Speech Audio Process.*, vol. 9, no. 5, pp. 504–512, Jul. 2001.

[26] I. Cohen and B. Bergdugo, "Noise estimation by minima controlled recursive for robust speech enhancement," *IEEE Signal Process. Lett.*, vol. 9, no. 1, pp. 12–15, Jan. 2002.

Huan WU received the B.Eng. degree from the Nanjing University of Aeronautics and Astronautics, Nanjing, China, in 2013, and the Ph.D. degree from The Chinese University of Hong Kong, Hong Kong, in 2018. She is currently a Postdoc Fellow with The Hong Kong Polytechnic University. Her current research interests include distributed optical fiber sensing and digital signal processing for sensing systems.

Chao Shang received the B.Eng. degree in electronic science and technology from Tianjin University in 2006, the M.Sc. degree in physical electronics and the Ph.D. degree in optical engineering from Beijing Jiaotong University in 2008 and 2013, respectively. He was a Research Associate at the Department of Electrical Engineering, Hong Kong Polytechnic University from 2017 to 2020. He is currently an Associate Professor with the School of Science, Beijing Jiaotong University. His current research interests include distributed optical fiber sensing and signal processing.

Kun ZHU received the B.A. and Ph.D. degrees from Zhejiang University, Hangzhou, China, in 2007 and 2012, respectively. He was a Research Engineer at the Central Research Institute of Huawei Technologies Co. Ltd. from 2012 to 2013. He was a Senior Research Associate at the City University of Hong Kong, Hong Kong from 2015 to 2016, and then as a Research Fellow from 2017 and 2019. Since 2020, he has been with both, the City University of Hong Kong and the Hong Kong Polytechnic University, as a Research Fellow. His research interests include microwave photonics, distributed fiber sensing systems, signal processing based on optical fiber, and waveguide devices.

Prof. Chao LU received the B.Eng. degree in electronic engineering from Tsinghua University, China in 1985, and the M.Sc. and Ph.D. degrees from the University of Manchester in 1987 and 1990 respectively. He joined the School of Electrical and Electronic Engineering, Nanyang Technological University(NTU), Singapore in 1991 and was there as a Lecturer, Senior Lecturer, and Associate Professor till 2006. From 2002 to 2005, he was seconded to the Institute for Infocomm Research, Agency for Science, Technology and Research (A*STAR), Singapore, as a Program Director and Department Manager leading a research group in the area of optical communication and fibre devices. He joined the Department of Electronic and Information Engineering, The Hong Kong Polytechnic University in 2006 and is a Chair Professor of Fibre Optics there now. Over the years, he has authored or coauthored more than 300 papers in major international journals. He has been an Organizer or a Technical Program Committee Member of many international conferences. His current research interests include the area of high capacity transmission techniques for long haul and short reach systems and distributed optical sensing systems. In addition to academic research work, he has had many industrial collaborative research projects and has a number of awarded patents. He is a Fellow of the Optical Society of America (OSA).